Current Science
CS 5 (4), 4001-4020 (2025)
Received 19 May 2025 | **Revised 18 June** 2025 | **Accepted 17 July**. 2025 | **Online Available 15 August** 2025
https://doi.org/ 10.52845/CS/2025-5-4-54

Current Science
Current Science

OPEN ACCESS

ISSN(O)2795-8639

Original Article

Differentially Expressed Genes and Their Signaling Pathways in ARPE-19 Cells Induced by 448 Nm Blue Light

Qiong Ma[#1], Tianchi Xu[#2], Yufang Cui[1], Changke Wang[1,3] Hongxiang Kang*[1]

[1]Beijing Institute of Radiation Medicine, Beijing, 100850, China,

[2]College of Life Sciences, Hebei University, Baoding, 071000, China,

[3]Wuhan National Laboratory for Optoelectronics, Huazhong University of Science and Technology, Wuhan, 430074, China

[*]Corresponding Author: Hongxiang Kang

Abstract:

The enduring exposure to blue light emerges as a potential contributor to retinal degenerative diseases, with damage to the retinal pigment epithelium identified as the primary source of light-induced retinal damage. This study delves into the detrimental effects of 448 nm blue light on human retinal pigment epithelial (ARPE-19) cells and the underlying mechanisms. ARPE-19 cells underwent irradiation with 25 mW/cm² of blue light for durations ranging from 3 to 12 hours. Comprehensive analyses, including transcriptome sequencing and RT-qPCR, were employed to assess alterations across different temporal groups. Following blue light exposure, the expression profile of ARPE-19 cells underwent significant changes. In the 6-hour group compared to the normal group, a total of 4894 differentially expressed genes (DEGs) were identified. Transcriptome sequencing analysis revealed an upregulation of apoptosis-related genes after 6-hours of blue light exposure. Correspondingly, RT-qPCR detection demonstrated that blue light could induce ferroptosis in ARPE-19 cells. Specifically, the expression levels of ferroptosis-related genes, including NCOA4, FTH1, FTL, SLC39A14, LPCAT3, HMOX1, SLC7A11, and P53, exhibited a significant increase, while the expression levels of SLC3A2 and GPX4 were significantly reduced. Blue light irradiation induced notable alterations in the cell expression profile, with ferroptosis occurring at the early stages of irradiation. The findings from this study provide valuable insights for the safe use of visible light laser. The paper should interest readers in the areas of laser-induced ocular damage, laser dazzling effects, and the development of laser dazzling devices.

1. Introduction

Changing lifestyles with less time spent outdoors and increasing use of light-emitting diodes (LEDs) have altered the pattern of blue light exposure in humans, which can expose humans to high levels of blue light (1-4). Prolonged or excessive exposure to blue light can have deleterious effects on the eye, especially the blue-violet band (380 to 450 nm), which can cross the cornea and lens to reach the retina, causing cumulative and long-lasting damage to retinal structures. Therefore, studies on blue light have focused on different blue-violet wavelengths, particularly 405 to 455 nm (5-8), with harmful effects peaking at 440 nm (9). Exposure to blue light encourages corneal epithelial cells to produce more reactive oxygen species (ROS), which in turn induces oxidative damage and apoptosis, leading to the development of dry eye (10). Absorption of blue light by the lens has a protective effect against potential retinal damage. However, this protective effect reduces lens transparency, potentially leading to cataract

formation, as blue light induces ROS production in the mitochondria of lens epithelial cells (hLECs) (11). Some studies suggest that blue light may accelerate age-related macular degeneration (AMD), especially after cataract surgery performed several years ago (12). In conclusion, the effect of blue light on the retina greatly affects people's normal life and has attracted much attention.

Currently, numerous studies investigate the effects of blue light on the retina, yet they remain subjects of ongoing debate. The retina, comprising five distinct cell layers, houses vital components such as rod cells, cone cells, and the retinal pigment epithelium (RPE), which plays a crucial role in maintaining retinal tissue's physiological function (13). Notably, RPE cells lack the capacity for proliferation and regeneration (14,15). Upon cell death, adjacent cells compensate by expanding and sliding, yet when the living cell count diminishes beyond compensation, RPE function is lost, severely affecting the retina's structure and function, ultimately causing retinal degenerative diseases. The retina, the primary absorber of visible wavelength light, is particularly susceptible to damage, especially RPE cells. Age-related macular degeneration (AMD), a disease of RPE cells, underscores the profound impact of RPE damage, making the understanding of blue-light-induced oxidative stress in RPE cells and subsequent RPE degeneration pivotal for preventing retinal damage (16). The mechanisms underlying retinal damage induced by blue light primarily encompass photothermal and photochemical damage, with the extent of damage contingent on irradiation intensity and duration (17,18). Numerous studies have demonstrated that prolonged exposure to short-wave blue light can result in damage to retinal pigment epithelial cells or photoreceptors, primarily through the mechanism of photochemical damage, leading to cell death; Excessive blue light exposure can lead to a variety of programmed cell deaths such as apoptosis, necrosis, and pyroptosis in RPE cells (19-21). Oxidative stress and apoptosis, mediated by the mitochondrial pathway, have been identified as pivotal mechanisms in blue light-induced damage to retinal cells.

Some studies indicated that excessive light exposure led to ferroptosis in RPE cells (22), but whether blue light can lead to ferroptosis in RPE cells and its related mechanism have not been reported. Ferroptosis, a form of programmed cell death (PCD) linked to the accrual of reactive oxygen species, is primarily characterised by the accumulation of iron ions and lipid peroxides. Dysregulation in cellular iron metabolism leads to the interaction of divalent iron ions with lipid peroxides, generating excessive ROS through the Haber Weiss and Fenton reactions. ROS subsequently reacts with unsaturated fatty acids on the cell membrane, generating numerous phospholipid peroxides, culminating in cell membrane disintegration and cell demise (23). Ferroptosis intricately ties into iron metabolism (24), lipid metabolism (25), amino acid metabolism (26), and the metabolic pathways of iron death-sensitive molecules, such as coenzyme Q10, p53, selenium, and vitamin E (27-29). In retinopathies stemming from excess all-trans-retinal (atRAL) accumulation, ferroptosis emerges as a significant pathway of photoreceptor cell death (30). Current evidence establishes that blue light pollution induces retinal damage and degeneration by activating ferroptosis (31).

To preclude the onset of retinal degenerative diseases and mitigate visual dysfunction associated with retinal light damage, it is imperative to elucidate the detrimental effects and underlying mechanisms of blue light irradiation on retinal pigment epithelium (RPE) cells. This study sought to establish a damage model within ARPE-19 cells through irradiation with 448 nm LED blue light. Notably, the conditions of RPE cells cultured in vitro cannot fully mimic the physiological environment in vivo, and RPE photosensizers like lipofuscin and melanin were not normally present in ARPE-19 cells. The resultant expression profile of ARPE-19 cells following blue light exposure was meticulously examined using eukaryotic reference transcriptome sequencing. Subsequently, an in-depth analysis encompassed differential gene functions, signalling pathway enrichment, and the construction of a protein interaction network. The study culminated in the application of RT-PCR to scrutinise potential programmed death modes within ARPE-19 cells subsequent to 448 nm LED blue light irradiation. This holistic approach aimed to identify differentially expressed genes, offering a fresh perspective and a theoretical foundation for extensive exploration into retinal

blue light injury, as well as advancements in disease prevention and treatment strategies.

Materials and Methods

Cell Culture

Human retinal pigment epithelial (ARPE-19) cells were purchased from the National Collection of Authenticated Cell Cultures in Shanghai, China, and were grown in Dulbecco's modified Eagle's medium F-12 (DMEM/F-12; Gibco Company, NY, USA) containing 10% fetal bovine serum (FBS) at 37 °C under a 5% CO_2 atmosphere.

Blue Light Irradiation Method

A bespoke blue light source was positioned within a controlled CO_2 cell culture incubator, specifically on the lower level. The LED blue light source, measuring 14 cm × 11 cm, emitted light with a peak wavelength of 448 nm and a full half-width of 18 nm. This LED source was powered by a mobile power supply. A transparent tempered glass bracket, vertically adjustable, secured the cell culture dish and regulated the vertical distance of blue light exposure. Cell culture plates were positioned directly above the light source's centre, directing blue light upwards towards the cells. Blue light intensity was precisely gauged using a laser power meter (Ophir Company, Jerusalem, Israel).

ARPE-19 cells, inoculated in 10 cm dishes at a density of 10^6 cells per millilitre, underwent a 12-hour incubation period in a dedicated cell culture incubator. Post-incubation, the cell culture plates were transferred to a blue light irradiation device, with power control facilitated by a power meter. Blue light exposure intensity was set at either 15 mW/cm^2 or 25 mW/cm^2, contingent on the cell plate area. Continuous irradiation lasting 3 to 12 hours ensued, with subsequent grouping of cells based on the duration of exposure. Following blue light exposure, cells were returned to the incubator for an additional 24 hours before subsequent testing. The normal control group comprised cells shielded from blue light exposure, maintained in a dark environment.

Observation of Cell Morphology and Activity Assay

ARPE-19 cells underwent irradiation with 15 mW/cm² and 25 mW/cm² of blue light for varying durations: 0, 3, 6, 9, and 12 hours. Immediate observations of cell morphology were conducted using an inverted microscope, followed by a subsequent 24-hour incubation period before the second observation. The 0-hour group served as the normal control without blue light exposure.

The non-fluorescent calcein acetylmethyl ester undergoes cleavage by intracellular esterase in living cells, transforming into green fluorescent calcein upon entry. This property makes it a suitable marker for detecting living cells. Post-blue light irradiation, the medium was aspirated, and 200 μL of a prepared calcein acetylmethyl ester working solution was added to both the normal and irradiated groups. Following a 20-minute incubation in the cell culture incubator, unbound staining reagents were washed out using phosphate-buffered saline (PBS). Subsequent observation under a fluorescence microscope revealed green fluorescence specifically in living cells, distinguishing them from non-viable counterparts.

Transcriptome Sequencing and Bioinformatics Analysis

ARPE-19 cells were subjected to blue light irradiation at 25 mW/cm² for durations of 0 hours, 6 hours, and 12 hours. Subsequently, the cells were cultured for an additional 24 hours before harvesting with a cell scraper. Cell samples underwent triple washes with phosphate-buffered saline (PBS), followed by TRIzol addition and loading into pre-cooled RNase-free cryopreservation tubes for rapid freezing with liquid nitrogen. The 0-hour group served as the normal control without blue light exposure, and three parallel samples were prepared in batches for each of the 0-hour, 6-hour, and 12-hour groups. Transcriptome sequencing was performed on these nine samples. RNA extraction, library construction for RNA sequencing, quality control, and sequencing were outsourced to Shanghai Majorbio Technology Co., Ltd. The protocol involved total RNA processing to prepare an mRNA sequencing (mRNA-seq) library using the Illumina TruSeq TM RNA Sample Prep Kit. Polyadenylated mRNAs were purified with poly-T oligo-coupled magnetic beads, followed by random fragmentation using a fragmentation buffer. First- and second-strand cDNAs were synthesized using reverse transcriptase, random primers, and DNA polymerase I. The resulting cDNA fragments underwent purification and enrichment through polymerase chain reaction

(PCR) to generate cDNA libraries, which were subsequently subjected to detection using a NextSeq500 sequencing system.The obtained imaging data were converted into sequence data and stored in FASTQ format. Sequence comparison software (version 2.1.0) facilitated the comparison of clean reads from each sample with the specific reference genome sequence, employing parameters of 125 bp seed comparison and allowing up to 2 mismatches per comparison. The aligned sequences were successively input into online software versions 2.1.2 (https://ccb.jhu.edu/software/stringtie/) 0.46.2 (https://pachterlab.github.io/kallisto/ download), and 1.24.0 (http://bioconductor.org/packages/ stats /bioc/DESeq2/)for transcript assembly, expression analysis, and expression difference analysis. Genes exhibiting an absolute fold change (FC) >2 and a false discovery rate (FDR) < 0.05 between groups (n=3) were identified as differentially expressed genes (DEGs). Further analyses included Gene Ontology (GO) significant enrichment analysis for DEGs using Goatools (version 0.6.5) online software, pathway analysis utilising Kyoto Encyclopedia of Genes and Genomes (KEGG) gene sets in the Ipath Database (version 3) online tool, and protein interaction network analysis through the String online tool and Cytoscape (version 3.9.1) software. Functional target genes were identified through these analyses.

Real-Time Quantitative PCR (RT–qPCR)

ARPE-19 cells underwent blue light irradiation at an intensity of 25 mW/cm² for varying durations: 0h, 3h, 6h, 9h, and 12h. Subsequently, the cells were cultured for an additional 24h before harvesting in an ice box using a cell scraper. Collection was performed in pre-cooled PBS buffer, and cellular RNA was subsequently extracted. The 0h group served as the normal control without blue light irradiation. Three parallel samples were meticulously prepared for each duration (0h, 3h, 6h, 9h, and 12h). RNA concentration was ascertained using an ultra-micro spectrophotometer, ensuring OD_{260nm}/OD_{280nm} values fell within the optimal range of 1.8 to 2.0. Extracted RNA was stored at -80°C for subsequent analyses. PCR primers for the amplification of human genes are detailed in Table 1.

Table 1. Primer sequences for RT-qPCR

Gene	Primer sequence (5'-3')	
NCOA4 (nuclear receptor co-activator 4)	Forward Reverse	GGAACCCAAACCTGAGC TGATAAGCCACTCCGACA
FTH1 (Ferritin heavy)	Forward Reverse	AGTCGTCGGGGTTTCCT GAGGGTGCGGTGAAGAG
FTL (Ferritin light)	Forward Reverse	GCCAACCAACCATGAGC GCGGTCGAAATAGAAGCC
SLC3A2 (Solute carrier family 3 member 2)	Forward Reverse	ATCAAGGTGGCGGAAGAC ATCAAGGTGGCGGAAGAC
SLC39A14 (Solute carrier family 39A14)	Forward Reverse	GTGTGGGGCTTTGGTTT CAGGGCGATGAAGTAAGTG
LPCAT3 (Lysophosphatidyl-choline acyltransferase 3)	Forward Reverse	TTCCAGATGGCCTACCTTC TCTTTCCCTCCGTCAAAGT
HMOX1 (heme oxygenase-1)	Forward Reverse	GTGACCCGAGACGGCTT ACAGGGGCGAAGACTGG
GPX4 (Glutathione peroxidase 4)	Forward Reverse	ATACGCTGAGTGTGGTTTGC CTTCATCCACTTCCACAGCG
P53 (tumor suppressor gene)	Forward Reverse	CCAGATGAAGCTCCCAGA GGGAAGGGACAGAAGATGA
SLC7A11 (Solute carrier family 7 member 11)	Forward Reverse	GAACGAGGAGGTGGAGAAT ACAGGTGAAAACTCAAAGGTG
GAPDH (glyceraldehyde-3-phosphate dehydrogenase)	Forward Reverse	CACCCACTCCTCCACCTTTG CCACCACCCTGTTGCTGTAG

Real-time PCR utilised TB Green® Premix Ex Taq™ II (Takara, Dalian, China) and analysis was conducted via the CFX OPUS 96 (Bio-Rad, Hercules, California, USA). The experimental protocol encompassed three programs: (1) Denaturation of the cDNA/RNA hybrid at 95°C for 30s; (2) Amplification of cDNA for 40 cycles, each cycle involving 95°C for 5s and 60°C for 30s; (3) Final cDNA amplification at 72 °C for 10min.

Statistical Analysis

The results were subjected to analysis using SPSS 13.0 software, presented as mean ± SD (standard deviation). Data were statistically analyzed using two-tailed Student's t-test. Values of $P<0.05$ were considered to indicate a significant difference.

Results

Observation of Cell Morphology after Blue Light Exposure

Figure 1 illustrates the morphological observations of ARPE-19 cells subjected to varying intensities of blue light exposure. Utilizing an inverted phase contrast microscope, the normal group displayed cells adhering well to the wall, assuming a spindle shape with clear and uniform borders. Following exposure to 15 mW/cm² blue light for 3~12 hours, the cell boundaries gradually blurred, and the number of scattered, round floating cells increased (Figure 1a). Remarkably, cell morphology essentially returned to normal after an additional 24-hour incubation post-blue light exposure. Elevating the intensity to 25 mW/cm² for 3~12 hours resulted in substantial changes in cell morphology compared to the normal group, with enlarged intercellular spaces and an increased number of floating cells (Figure 1b). Notably, the 9~12 hours exposure period led to a significant rise in floating cells. However, 24 hours post-exposure, the 3h group cells reverted to normal, the 9h group witnessed a considerable decrease in adherent cells with some floating cells, and the 12h group exhibited poor cell morphology, characterized by a plethora of floating cells and cell fragments with few adherent cells. The findings affirm that the morphology of ARPE-19 cells remained largely unchanged 24 hours after 15 mW/cm² blue light exposure. In contrast, significant alterations in cell morphology were evident 24 hours after exposure to 25 mW/cm² blue light, particularly in the 9h and 12h groups. Consequently, the 25 mW/cm² blue light exposure dose was adopted as the damage-inducing dose for subsequent experiments on RPE cells.

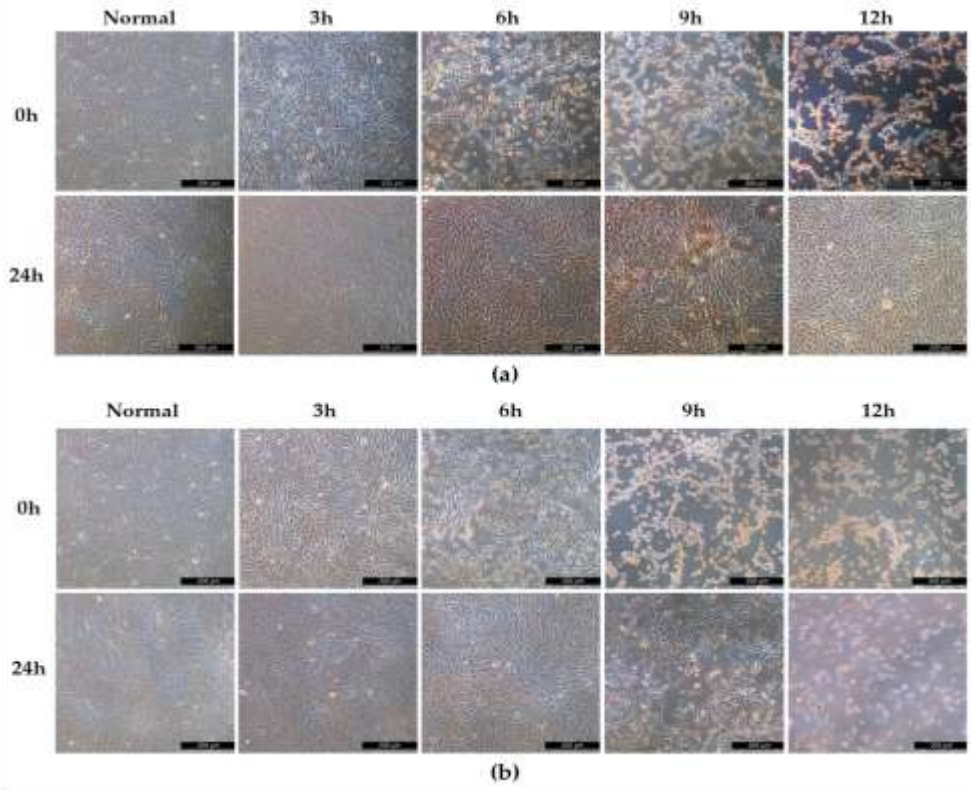

Figure 1. The morphological changes of ARPE-19 cells after blue light exposure at different

intensities. (a) Cell morphological changes 0h and 24h after 15 mW/cm2 blue light exposure. (b) Cell morphological changes 0h and 24h after 25 mW/cm2 blue light exposure.

Activity of ARPE-19 cells after Blue Light Exposure

ARPE-19 cells were irradiated with 25mW/cm^2 blue light for 3~12 h, and the results of cell staining were shown in Figure 2. The cells in the unirradiated group were well adhered to the wall and were basically live cells with green fluorescence. In the 3h group, the cell morphology started to become blurred. In the 6h group, cell gaps began to appear, and some unstained dead cells existed. 9h and 12h groups showed significant changes in cell morphology, which were mainly manifested by cell swelling, increased cell gaps, significantly increased number of floating cells and increased cell debris, and a large number of unstained dead cells were observed.

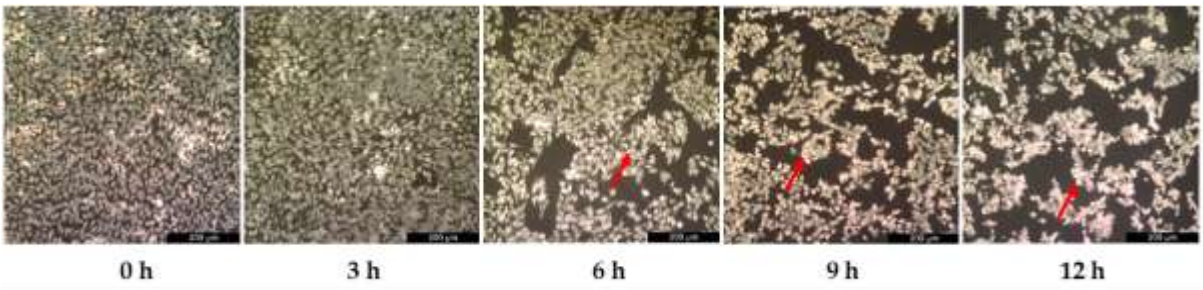

Figure 2. **The effects on the activity of ARPE-19 cells after 25 mW/cm^2 blue light exposure for 3~12 h. The red arrows denoted dead cells without fluorescent staining.**

Statistics and Analysis of Differentially Expressed Genes after Blue Light Exposure

Transcriptome sequencing was conducted on the 6-hour group (mild injury) and the 12-hour group (severe injury) exposed to 25 mW/cm² blue light to scrutinize the alterations in the expression profile of ARPE-19 cells under blue light exposure. The sequencing outcomes unveiled a significant transformation in the expression profile of ARPE-19 cells post-blue light exposure. In the 6-hour group, there were 4894 differentially expressed genes (DEGs), with 2572 upregulated and 2322 downregulated genes compared to the normal group. In the 12-hour group, 5012 DEGs were identified, comprising 2874 upregulated and 2138 downregulated genes in comparison with the normal group. Notably, there were 166 DEGs (120 upregulated and 46 downregulated) when comparing the 12-hour group to the 6-hour group, as illustrated in the volcano diagram depicted in Figure 3. Moreover, the number of upregulated DEGs exceeded that of downregulated DEGs. Detailed statistics of DEGs for the three groups, along with the top 20 upregulated and downregulated DEGs, are presented in Tables 2-5.

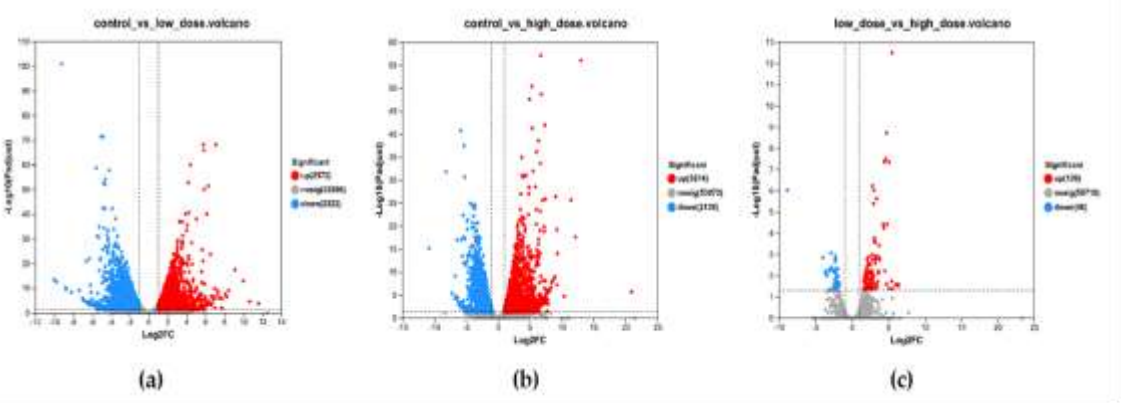

Figure 3. **Volcano plots of DEGs in the normal group, 6-hour group and 12-hour group. (a) DEGs in the 6-hour group vs. the normal group; (b) DEGs in the 12-hour group vs. the normal group; DEGs in the 6-hour group vs. the 12-hour group**

Table 2. The number of DEGs in the three different groups.

Different groups	Total	Up-regulation	Down-regulation
The 6-hour group vs. the normal group	4894	2572	2322
The 12-hour group vs. the normal group	5012	2874	2138
The 12-hour group vs. the 6-hour group	166	120	46

[1] The screening threshold was$|\log_2 FC| \geq 1$, p-value < 0.05, padjust < 0.05; FC: fold change.

Table 3. The DEGs in the 6-hour group vs. the normal group (|log2 FC| sorting before 20)

Upregulated DEGs			Downregulated DEGs		
Gene	**$\log_2$FC**	**p-value**	**Gene**	**$\log_2$FC**	**p-value**
SLC30A2	11.61	2.39E-05	AC087721.2	-10.00	5.34E-16
STK32A	10.65	2.43E-06	AC087190.3	-9.73	5.28E-15
DUSP15	9.97	1.72E-15	NPPB	-9.22	7.07E-106
HSPA6	9.11	2.68E-20	EDN2	-8.76	1.61E-12
ATP6V0D2	8.44	3.49E-11	AC103718.1	-8.74	1.03E-11
C2CD4A	8.25	2.09E-08	AF127577.4	-8.21	1.73E-10
AP003392.3	8.09	1.46E-09	MIR137HG	-7.36	2.23E-11
SLC9A2	7.75	1.46E-07	SEMA3E	-7.00	7.68E-08
DLL4	7.71	3.68E-03	AL133325.3	-6.92	5.53E-07
SNORD3B-1	7.67	7.02E-08	CRNN	-6.86	1.01E-06
IFI30	7.67	1.92E-03	FAM83A	-6.78	1.29E-06
RASD1	7.36	8.02E-08	FAM111B	-6.64	7.06E-24
RAB7B	7.35	7.72E-08	AC112777.1	-6.53	5.24E-06
SLC16A9	7.30	9.30E-10	CLDN22	-6.40	1.36E-05
MYCL	7.23	3.51E-11	DNAAF4-CCPG1	-6.38	8.43E-05
SLC16A14	7.09	1.83E-72	LINC01936	-6.34	2.28E-06
DUSP26	6.97	1.92E-03	VXN	-6.32	1.75E-05
GADD45G	6.95	3.88E-12	AL161891.1	-6.30	1.94E-05
KCNK3	6.93	1.35E-08	LINC00968	-6.29	4.90E-25
EPHB6	6.88	2.39E-07	AC021016.3	-6.26	2.61E-05

Table 4. The DEGs in the 12-hour group vs. the normal group (|$\log_2$ FC| sorting before 20)

Up-regulated gene			Down-regulated gene		
Gene	**$\log_2$FC**	**p-value**	**Gene**	**$\log_2$FC**	**p-value**
AC0045282	20.95	8.49E-08	TMEM203	-10.82	3.58E-18
HSPA6	12.96	9.98E-61	MIR210HG	-8.15	1.23E-35
RASD1	12.14	9.41E-21	AL139099.1	-7.22	1.88E-07
NGFR	11.43	3.07E-29	AC027796.3	-6.76	4.52E-06
IFI30	10.38	1.04E-06	CAVIN2	-6.71	1.23E-11
GADD45G	9.31	5.63E-17	AUXG01000058.1	-6.69	3.67E-06
RGS16	9.22	1.85E-22	AC003958.2	-6.61	7.77E-07
DUSP15	9.22	1.89E-09	NPPB	-6.421	4.38E-20
PGF	9.01	5.33E-30	MNS1	-6.32	3.31E-06
CD14	8.95	2.19E-11	AC112777.1	-6.26	3.78E-05
DLL4	8.65	1.06E-10	POLR2J2	-6.14	1.07E-04
HEY2	8.36	4.68E-10	AC016394.2	-6.10	7.74E-05
AL121758.1	8.29	6.52E-09	HPDL	-6.09	9.82E-05
SNORD3B-1	8.13	3.47E-08	CYP24A1	-5.85	7.59E-45
SLC16A9	7.89	1.03E-04	AC245060.5	-5.84	2.49E-04

CASS4	7.89	1.02E-07	AP000295.1	-5.83	8.52E-04
COL20A1	7.79	8.77E-06	E2F8	-5.82	4.07E-05
PCDH19	7.71	2.73E-08	STARD4-AS1	-5.78	3.63E-20
RSAD2	7.71	6.97E-03	TTC3P1	-5.72	8.40E-05
AL139246.3	7.62	1.33E-07	EDN2	-5.62	2.45E-16

Table 5. The DEGs in the 12-hour group vs. the 6-hour group (|log_2 FC| sorting before 20)

Up-regulated gene			**Down-regulated gene**		
Gene	**Log_2FC**	**p-value**	**Gene**	**Log_2FC**	**p-value**
HIST2H4B	6.37	2.42E-04	TMEM203	-8.87	4.89E-10
ZCCHC12	6.32	1.89E-04	GAREM2	-3.99	2.21E-06
NPIPB7	5.95	2.23E-04	KCNK3	-3.69	3.09E-05
AC010327.4	5.56	4.48E-04	IL1β	-3.54	1.98E-05
RGS16	5.49	2.02E-17	LCMT2	-3.44	4.64E-05
HIST1H2AG	5.43	1.15E-04	EGR1	-3.11	2.01E-05
ARC	5.09	1.33E-11	ITGA2	-2.98	4.76E-04
RPSAP58	5.08	3.89E-04	CCDC71	-2.89	9.99E-07
CD14	4.80	2.60E-08	CDK5R2	-2.86	1.02E-05
KRT8P50	4.74	1.86E-04	AC009237.14	-2.74	1.41E-05
RASD1	4.73	2.43E-13	CSTF2T	-2.49	2.21E-05
ANKRD1	4.61	6.40E-12	PIGM	-2.49	3.77E-04
AC093525.2	4.51	1.82E-05	NHLRC1	-2.48	2.69E-04
PGF	4.45	1.41E-11	SLITRK5	-2.46	2.76E-04
CDKN1C	4.39	4.71E-08	TMEM102	-2.41	2.38E-05
RND1	4.28	2.99E-08	FAM155B	-2.39	1.98E-04
HSPA6	3.81	3.22E-06	AC009237.3	-2.38	1.61E-04
RN7SK	3.80	2.79E-06	JRK	-2.34	2.68E-05
CCNE2	3.73	4.20E-07	MRM1	-2.34	8.41E-05
CCDC121	3.65	2.01E-05	CBX7	-2.33	4.47E-06

Genes sharing similar expression patterns often exhibit functional relevance. Therefore, an expression pattern clustering analysis of genes within the selected gene set was executed. This involved calculating sample distances based on gene expression levels and subsequent sample classification through an iterative method. The outcomes showcased high repeatability among the normal group, 6-hour exposure group, and 12-hour exposure group. The correlation between samples within the same group was substantial, and a noticeable distinction in overall gene expression levels was evident among the three groups, as depicted in Figure 4.

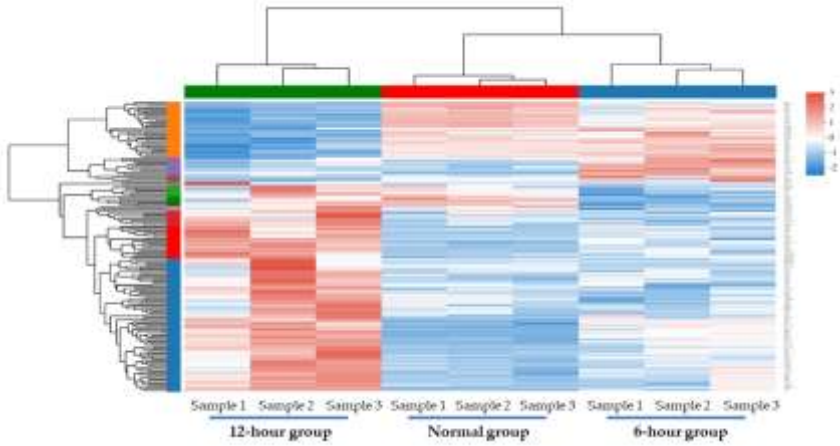

Figure 4. **Clustering heatmap analysis of DEGs in the normal group, 6-hour group and 12-hour group.**

Note: each column in the figure represents one sample, and each row represents one gene; red indicates that the level of gene expression in the sample was high, and blue indicates that the level of expression was low. For the specific change trend in expression levels, please refer to the number label under the color bar at the top right. The left side is the gene cluster tree, and the right side is the gene

Venn Diagram Analysis of DEGs

Venn analysis provides a comprehensive overview of the experimental data, examining intersections between different groups. This analysis reveals the number of genes in each differential set and elucidates the relationships between genes in these sets. The findings demonstrated that 56 differentially expressed genes were consistently present in cells from the normal group, as well as in those exposed to blue light for 6 and 12 hours. Among these genes, 46 exhibited a continuous upregulation, 4 displayed a sustained downregulation, 3 initially decreased and later increased, while 3 demonstrated an initial increase followed by a decrease, as visually represented in Figure 5. Detailed information for these 56 differentially expressed genes can be found in Table 6.

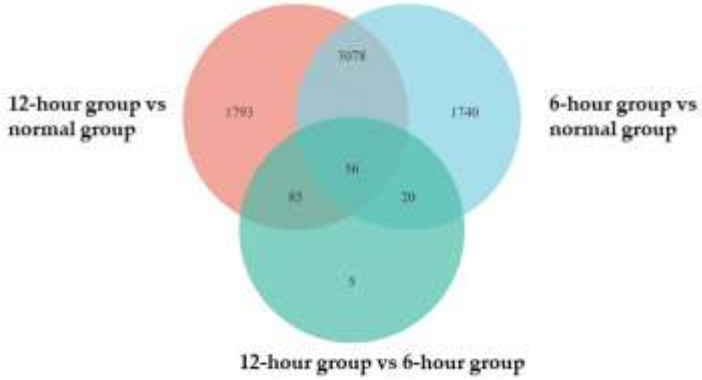

Figure 5. Venn diagram of DEGs in the normal group, 6-hour group and 12-hour group. Note: the circles with different colors represent different gene sets, and the numerical value represents the number of shared or unique genes among different gene sets

Table 6. Information on 56 DEGs with persistent expression.

Gene ID	Gene name	Gene description
ENSG00000007944	MYLIP	myosin regulatory light chain interacting protein
ENSG00000028839	TBPL1	TATA-box binding protein like 1
ENSG00000051108	HERPUD1	homocysteine inducible ER protein with ubiquitin like domain 1
ENSG00000070495	JMJD6	jumonji domain containing 6, arginine demethylase and lysine hydroxylase
ENSG00000087074	PPP1R15A	protein phosphatase 1 regulatory subunit 15A
ENSG00000103550	KNOP1	lysine rich nucleolar protein 1
ENSG00000105085	MED26	mediator complex subunit 26
ENSG00000108551	RASD1	ras related dexamethasone induced 1
ENSG00000115738	ID2	inhibitor of DNA binding 2
ENSG00000119508	NR4A3	nuclear receptor subfamily 4 group A member 3
ENSG00000119630	PGF	placental growth factor
ENSG00000120738	EGR1	early growth response 1
ENSG00000124216	SNAI1	snail family transcriptional repressor 1
ENSG00000130054	FAM155B	family with sequence similarity 155 member B
ENSG00000132002	DNAJB1	DnaJ heat shock protein family (Hsp40) member B1
ENSG00000135111	TBX3	T-box 3
ENSG00000138670	RASGEF1B	RasGEF domain family member 1B

ENSG00000141582	CBX4	chromobox 4
ENSG00000143315	PIGM	phosphatidylinositol glycan anchor biosynthesis class M
ENSG00000143333	RGS16	regulator of G protein signaling 16
ENSG00000148926	ADM	adrenomedullin
ENSG00000151929	BAG3	BCL2 associated athanogene 3
ENSG00000153094	BCL2L11	BCL2 like 11
ENSG00000153487	ING1	inhibitor of growth family member 1
ENSG00000158050	DUSP2	dual specificity phosphatase 2
ENSG00000163273	NPPC	natriuretic peptide C
ENSG00000163376	KBTBD8	kelch repeat and BTB domain containing 8
ENSG00000163806	SPDYA	speedy/RINGO cell cycle regulator family member A
ENSG00000167772	ANGPTL4	angiopoietin like 4
ENSG00000170385	SLC30A1	solute carrier family 30 member 1
ENSG00000170458	CD14	CD14 molecule
ENSG00000171401	KRT13	keratin 13
ENSG00000172602	RND1	Rho family GTPase 1
ENSG00000173110	HSPA6	heat shock protein family A (Hsp70) member 6
ENSG00000174010	KLHL15	kelch like family member 15
ENSG00000175197	DDIT3	DNA damage inducible transcript 3
ENSG00000176714	CCDC121	coiled-coil domain containing 121
ENSG00000176842	IRX5	iroquois homeobox 5
ENSG00000178381	ZFAND2A	zinc finger AN1-type containing 2A
ENSG00000182580	EPHB3	EPH receptor B3
ENSG00000187713	TMEM203	transmembrane protein 203
ENSG00000197329	PELI1	pellino E3 ubiquitin protein ligase 1
ENSG00000197933	ZNF823	zinc finger protein 823
ENSG00000198417	MT1F	metallothionein 1F
ENSG00000198576	ARC	activity regulated cytoskeleton associated protein
ENSG00000198890	PRMT6	protein arginine methyltransferase 6
ENSG00000203812	HIST2H2AA3	histone cluster 2 H2A family member a3
ENSG00000204103	MAFB	MAF bZIP transcription factor B
ENSG00000204388	HSPA1B	heat shock protein family A (Hsp70) member 1B
ENSG00000204389	HSPA1A	heat shock protein family A (Hsp70) member 1A
ENSG00000204516	MICB	MHC class I polypeptide-related sequence B
ENSG00000205189	ZBTB10	zinc finger and BTB domain containing 10
ENSG00000227766	AL671277.1	HLA complex group 4 pseudogene 5
ENSG00000234616	JRK	Jrk helix-turn-helix protein
ENSG00000273734	AC005258.1	novel protein, readthrough between OAZ1 and SPPL2B
ENSG00000285565	AL671762.1	novel transcript

Significant Enrichment Analysis of DEGs

Conducting a thorough functional enrichment analysis on the genes within the differential gene set, encompassing both Gene Ontology (GO) and Kyoto Encyclopedia of Genes and Genomes (KEGG) analyses, provides insights into the principal functions and metabolic signalling pathways involved. A total of 2572 upregulated genes and 2322 downregulated genes were identified between the 6-hour exposure group and the normal group. GO analysis unveiled that upregulated genes were predominantly associated with oxidative stress, metabolic regulation, and signal transduction processes (Figure 6a). Conversely, downregulated genes primarily participated in cell proliferation (Figure 6b). Meanwhile, KEGG pathway enrichment analysis of upregulated genes highlighted augmented cell membrane component catabolism, activation of

diverse immune signalling pathways, and the apoptotic cascade (Figure 6c), including Notch, MAPK, and mTOR signalling pathways. Downregulated genes were primarily implicated in DNA damage repair and amino acid biosynthesis (Figure 6d). Similarly, between the 12-hour exposure group and the 6-hour group, 120 upregulated genes and 46 downregulated genes were identified. GO analysis indicated that upregulated genes were mainly involved in temperature response and metabolic regulation of compounds (Figure 6e), while downregulated genes were associated with small RNA metabolism, modification, and oxygen level response (Figure 6f). KEGG analysis demonstrated that upregulated genes participated in immune signalling pathways and apoptosis processes (Figure 6g), such as MAPK and NF-κB signalling pathways. Conversely, downregulated genes were primarily linked to various immune signalling pathways, compound metabolism, and synthesis processes (Figure 6h), including Toll-like receptor, TNF, C-type lectin receptor, and NOD-like receptor signalling pathways.

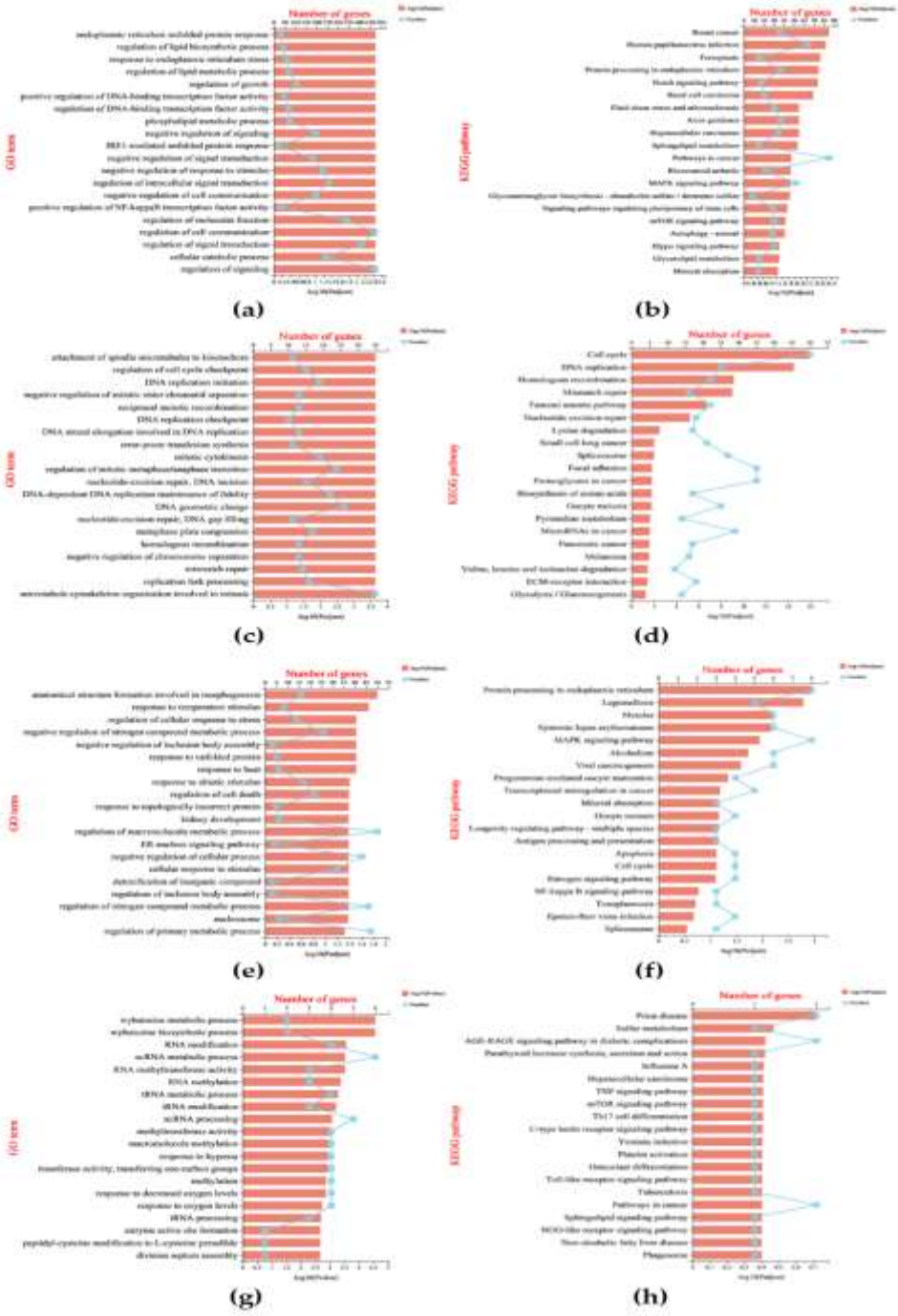

Figure 6. Significant enrichment analysis of DEGs. (a)~(b) GO and KEGG enrichment analyses of

upregulated genes in the 6-hour group vs. the normal group. (c)~(d) GO and KEGG enrichment analyses of downregulated genes in the 6-hour group vs. the normal group. (e)~(f) GO and KEGG enrichment analyses of upregulated genes in the 12-hour group vs. the 6-hour group. (g)~(h) GO and KEGG enrichment analysis of downregulated genes in the 12-hour group vs. the 6-hour group. Note: the enrichment results were the top 20 results under the condition of padjust<0.5, and the smaller the padjust was, the larger the value of -log10 (padjust) was, and the more significant the enrichment of GO terms and KEGG pathways was.

Protein Interaction Network Analysis of DEGs

Proteins conventionally assemble into complexes through interactions, subsequently executing specific functions. By delving into protein interaction network analysis, differentially expressed genes demonstrating interactions typically share functional similarities. This analysis aids in pinpointing potential differentially expressed genes, facilitating subsequent homology alignment of genes linked to protein interactions. Notably, target proteins such as cyclin B1 (CCNB1), minichromosome maintenance protein 4 (MCM4), minichromosome maintenance protein 2 (MCM2), and cell division cyclin 6 (CDC6) may assume pivotal roles in blue light exposures lasting less than 6 hours, as depicted in Figure 7a. Conversely, target proteins including interleukin 1β (IL-1β), early growth response protein 1 (EGR1), DNA damage-inducing transcription factor 3 (DDIT3), and heat shock protein A1A (HSPA1A) emerge as significant players within the exposure timeframe ranging from 6 to 12 hours, as illustrated in Figure 7b.

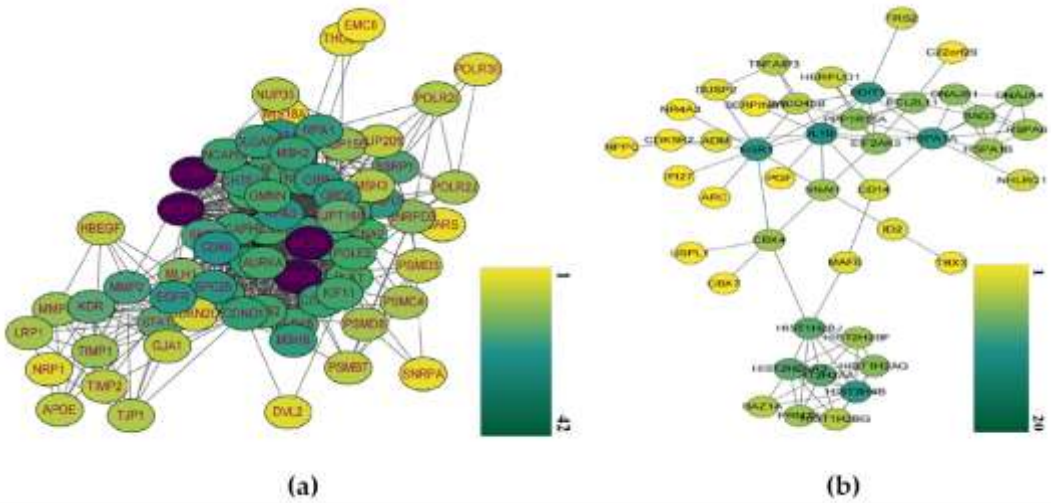

(a) (b)

Figure 7. Interaction network analysis of DEGs and proteins in the three groups. (a) Interaction network analysis in the 6-hour group and normal group; (b) Interaction network analysis in the 12-hour group and 6-hour group. (Legend: The line in the network diagram represents the regulatory relationship between genes; purple represents the gene most closely related to other genes in the network, with the most important function; green is the second; and yellow is the weakest)

Validation of RNA-seq Results

Ferroptosis, a recently uncovered iron-dependent cell death mechanism triggered by lipid peroxidation, stands apart from apoptosis, characterized by distinctive traits such as iron accumulation and lipid peroxidation. Intimately linked with iron metabolism, lipids, and amino acids, ferroptosis was observed in ARPE-19 cells exposed to 6-hour blue light in our prior transcriptome sequencing experiments. Subsequent RT–PCR analysis targeted 10 ferroptosis-related genes in ARPE-19 cells following blue light exposure. The detected expression changes in nuclear receptor coactivator 4 (NCOA4), ferritin heavy chain (FTH1), ferritin light chain (FTL), cyst amino acid and glutamate transfer protein heavy chain (SLC3A2), solute carrier family 39 (SLC39A14), lysolecithin acyltransferase 3 (LPCAT3), heme oxygenase 1

(HMOX1), glutathione peroxide enzyme 4 (GPX4), tumor suppressor gene (P53), and cystine and glutamate transfer protein light chain (SLC7A11) affirm that blue light serves as an inducer of ferroptosis in ARPE-19 cells. Comparative analysis with the normal group revealed a significant upregulation in the expression levels of iron metabolism-related genes (NCOA4, FTL, FTH1, and SLC39A14) and a notable downregulation in amino acid metabolism-related genes (SLC3A2 and SLC7A11) in the 3-hour group (Figure 8a~f). Similarly, lipid metabolism-related genes (LPCAP3, P53, and HMOX1) demonstrated a substantial upregulation, whereas GPX4 displayed a significant decrease in expression levels in the 6-hour group (Figure 8g~i). These outcomes strongly suggest the induction of ferroptosis in ARPE-19 cells upon exposure to blue light.

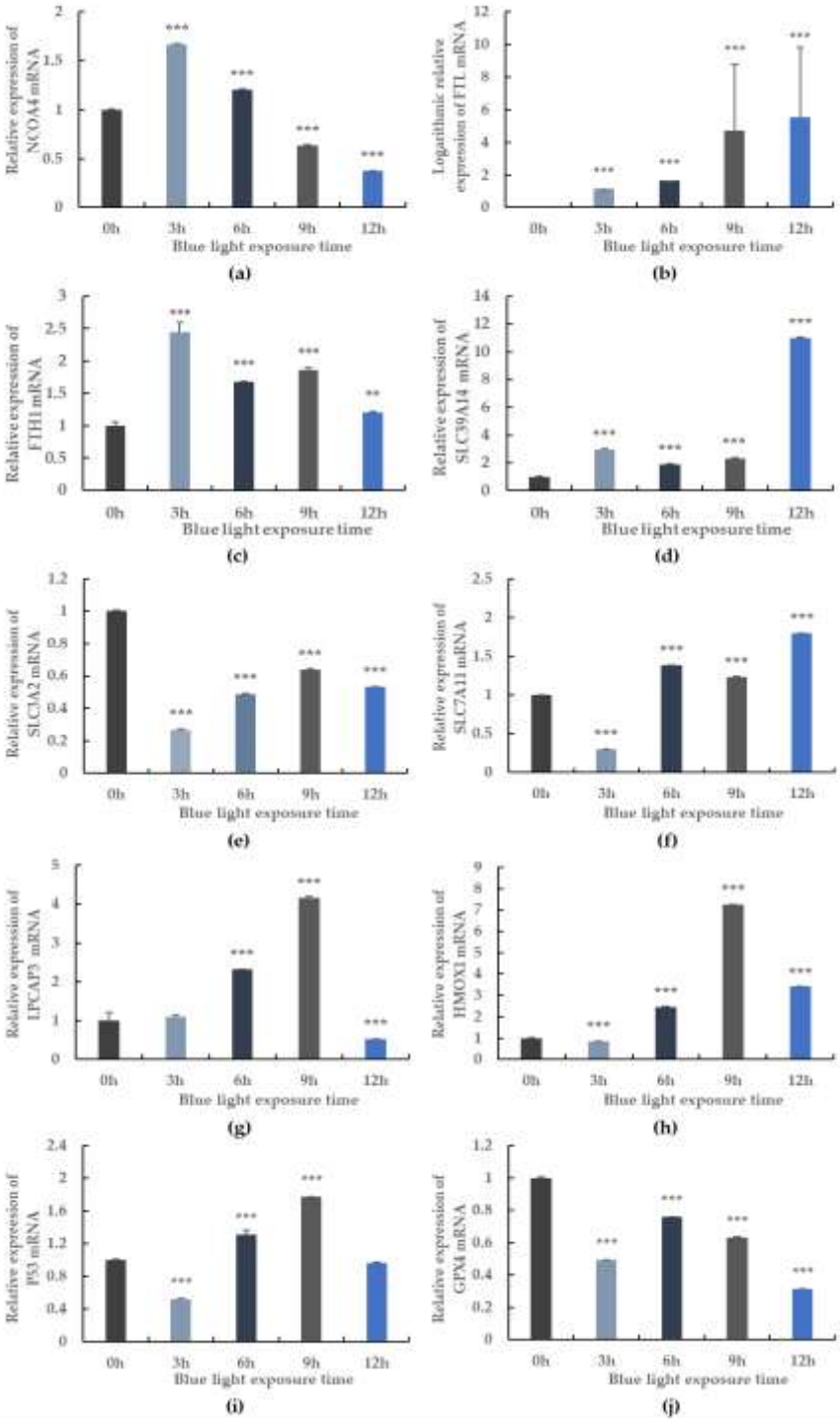

Figure 8. RT–PCR was used to detect the effect of blue light on the expression of ferroptosis-related genes in ARPE-19 cells. (a)~(d) The expression levels of the iron metabolism-related genes NCOA4,

FTL, FTH1, SLC39A14; (e)~(f) The expression levels of the amino acid metabolism-related genes SLC3A2, SLC7A11; (g)~(j) The expression levels of the lipid metabolism-related genes LPCAP3, P53, HMOX1, GPX4.Preferred formats are: EPS or PDF for line art or combination images, TIFF for photographic images. Office formats may be acceptable but the printed result cannot be guaranteed.

Discussion

The pervasive use of LED light sources in daily life prompts growing concern about their potential adverse effects on human health. Extensive exposure to daylight or LED light sources has been substantiated to inflict irreversible harm on the human retina, culminating in retinal degenerative diseases. The LED exposure time is highly variable between studies, ranging from constant exposures of 2 to 72 h to cyclic exposures of 3 to 12 h per day; Light intensity has also varied from 150 lux to 6000 lux; The periods of analysis of the effects of light on the retina also vary from 0d to 7d after phototoxic damage (32). Of particular concern is shortwave blue light, with its elevated energy levels and potent ability to induce active oxygen production in cells, posing a threat to human well-being. Situated in the outermost retinal layer, the retinal pigment epithelium (RPE) harnesses melanin-rich pigments to absorb light, averting photodamage, and substantiates its pivotal role in sustaining visual function and the visual cycle (33). Therefore, elucidating the photodamage mechanism in RPE cells assumes paramount significance.

In this study, an LED blue light model utilising a 448 nm wavelength irradiated ARPE-19 cells at intensities of 15 mW/cm^2 and 25 mW/cm^2 to elicit cell damage and instantiate a light damage model. Outcomes unveiled pronounced alterations in ARPE-19 cell morphology-contraction, swelling, rounding, cell gaps, and floating cells-linked intricately to light duration. Remarkably, cells subjected to 15 mW/cm^2 blue light recuperated to normal growth states within 24 hours, rendering this intensity suboptimal for establishing a light damage model. Conversely, cells exposed to 25 mW/cm^2 blue light for 24 hours exhibited diverse states; the 3-h and 6-h groups manifested negligible changes, while the 9-h and 12-h groups exhibited significant alterations, notably increased nonadherent cells, with the latter group displaying more profound changes. Consequently, the light damage model predicated on 25 mW/cm^2 was deemed more favourable. Concurrently, cell viability experiments substantiated a substantial reduction in viable cells in the 6h, 9h, and 12h groups following 25 mW/cm^2 blue light exposure. This reduction intensified with prolonged irradiation time, aligning with findings from analogous studies.

Eukaryotic transcriptome sequencing refers to the sequencing of species with reference genes. Compared with traditional sequencing technology, it has many unique advantages, such as a wide detection range, fast sequencing, high sensitivity, high accuracy, low cost, and simple operation (34). Extended exposure to blue light induces oxidative stress in the retina, resulting in severe damage to retinal tissues, particularly the retinal pigment epithelium (RPE) cells. Given the continuous photochemical reactions in the retina for vision, it consistently consumes substantial oxygen, undergoing oxidation for energy production. Blue light stimulation intensifies the generation of free radicals by retinal mitochondria, causing functional impairment and eventual death of RPE and photoreceptor cells. This oxidative stress response may activate pro-inflammatory factors and immune signaling pathways (35). Transcriptome sequencing in this study unveiled substantial changes in the gene expression profile of ARPE-19 cells under continuous blue light irradiation. A comparison with the normal group revealed 4894 differentially expressed genes (DEGs) in the 6-hour blue light exposure group and 5012 DEGs in the 12-hour exposure group. Additionally, 166 DEGs were identified in the 12-hour irradiation group compared with the 6-hour group, with 56 genes showing sustained differential expression in both irradiation groups. GO and KEGG enrichment analyses shed light on the functions and metabolic pathways affected by the upregulated and downregulated DEGs. The findings indicated that 6 hours of blue light irradiation induced oxidative stress, DNA damage, and activation of immune signaling pathways (NF-κB, Notch, MAPK, and mTOR) in ARPE-19 cells. Particularly, KEGG enrichment analysis of upregulated DEGs suggested potential involvement of autophagy and ferroptosis in cellular responses. The cell culture

medium temperature exhibited a nonsignificant increase at 6 hours post-exposure but rose approximately 2℃ at 12 hours post-exposure. Consequently, the heightened heat stress response led to diminished cell tolerance, evident in the inhibition of various immune signal transduction pathways (Toll-like receptor, TNF, C-type lectin, and NOD-like receptor). Simultaneously, multiple apoptotic pathways were likely initiated, ultimately resulting in membrane dissolution and cell death. Protein interaction network analysis identified DNA damage-inducing transcription factor 3 (DDIT3) and heat shock protein A1A (HSPA1A) as crucial target proteins in severe cell damage induced by blue light. Notably, the study by Xie C et al. (36) revealed LC3B downregulation in mouse RPE following early-stage LED light exposure, hinting at its involvement in retinal degeneration. Autophagy, besides ferroptosis, emerges as a significant mechanism for RPE cell injury induced by light exposure, opening avenues for future investigations into retinal photodamage.

This investigation identified morphological changes reminiscent of ferroptosis in ARPE-19 cells, including cell swelling and membrane rupture, occurring 6~12 hours post blue light irradiation. Transcriptome sequencing revealed upregulated expression of apoptosis-related genes in the 6-hour blue light exposure group. Moreover, gene RNA-seq experiments confirmed blue light-induced ferroptosis in ARPE-19 cells, evidenced by the significant upregulation of ferroptosis-related genes (NCOA4, FTH1, FTL, SLC39A14, LPCAT3, HMOX1, SLC7A11, and P53) and downregulation of SLC3A2 and GPX4. Tang Z et al. (37) similarly identified HMOX1 and SLC7A11 as dramatically upregulated genes in NaIO3-treated RPE cells, associating RPE degeneration with HO-1-regulated ferroptosis (38). NCOA4, a pivotal regulator of cellular iron balance, interacts with ferritin heavy chain, promoting ferritin degradation and iron ion concentration elevation (39). SLC39A14, responsible for ferrous ion transport (40), and ferritin chains (FTH1, FTL) play roles in regulating intracellular iron levels (41). Consequently, 6 hours of blue light irradiation significantly increased NCOA4, FTH1, FTL, and SLC39A14 expression, collectively inducing ferroptosis by elevating iron ion and reactive oxygen species concentrations. Post 6-hour blue light exposure, increased expression of tumour suppressor P53, LPCAT3 (facilitating lipid peroxide formation from unsaturated fatty acids), and HMOX1 (heme degradation into free iron) further supported ferroptosis induction. GPX4, a crucial antioxidant enzyme (42,43), inhibits ferroptosis by catalysing the conversion of lipid peroxide peroxide groups into hydroxyl groups using glutathione as a reducing agent (44). Notably, reduced expression of SLC7A11, SLC3A2, and GPX4 after 3 hours of blue light irradiation promoted ferroptosis in ARPE-19 cells. Chen C et al. (30) confirmed ferroptosis in the neural retina of Abca4-/-Rdh8-/-mice post light exposure, suggesting its role in photoreceptor cell death in retinopathies with excess atRAL accumulation. Investigating the presence of light exposure-induced ferroptosis in dry age-related macular degeneration (AMD) and Stargardt disease (STGD1) mice is a crucial future direction. In another study, we found that 25 mW/cm^2 blue light irradiation for 9-12 h induced necroptosis in ARPE-19 cells. Compared with the normal group, the expression levels of the necroptosis-related genes receptor-interacting protein kinase 1(RIPK1) and receptor-interacting protein kinase 3 (RIPK3) were significantly higher after 3~9 hours of blue light exposure, and reached the maximum value at 9 h of irradiation; The expression levels of necroptosis-related proteins RIPK1, RIPK3 and P-MLKL significantly increased with the increase of irradiation time after 6~12 hours of blue light exposure, and reached the maximum value at 12 h of irradiation (45). Moreover, the occurrence of necroptosis may be related to the degree of DNA damage. Song W et al. demonstrated that blue light-induced ARPE-19 cell death was necroptosis rather than apoptosis (46). A recent study found that blue light triggered apoptosis in an intensity-dependent manner in RPE cells isolated from Sprague-Dawley (SD) rats (47). Earlier studies found that low-luminance blue light induced apoptosis in ARPE-19 cells via the Bax/Bcl-2 pathway (48). In summary, the type of apoptosis in different RPE cells caused by blue light exposure needs further study.

Notably, RPE photosensizers like lipofuscin and melanin were not normally present in ARPE-19 cells. Blue light interacts with RPE-associated photosensitisers such as lipofuscin and melanin,

as well as photoreceptor-associated photosensitisers (e.g., proteins and retinol), to cause cellular damage (49). A2E serves as a important mediator of blue light-induced RPE cell damage, initiating a cell death program executed by a proteolytic caspase cascade, and regulated by Bcl-2 (50). Several studies have used A2E-loaded RPE cells to investigate the mechanism of blue light-induced damage to these cells (51,52). In addition, the DMEM/F-12 medium used in this experiment contains riboflavin and a relatively high iron concentration, potentially mediating blue light-induced phototoxicity via singlet oxygen and superoxide production (53). In summary, based on these two limitations in this study, animal studies are imperative to validate and explore further mechanisms involved in blue light-induced retinal damage.

Conclusions

Damage was induced in ARPE-19 cells through 448 nm blue light irradiation for 3-12 hours, with the severity escalating in proportion to the irradiation intensity and duration. Profound alterations in the expression profile of ARPE-19 cells were observed following blue light exposure. A total of 2572 upregulated and 2322 downregulated genes were identified between the 6-hour group and the normal group. This suggests that cells triggered a stress regulation program post-blue light irradiation, activating immune signaling pathways like Notch, MAPK, and mTOR. Concurrently, DNA damage repair mechanisms weakened, potentially leading to autophagy or ferroptosis in cells. Verification confirmed the induction of ferroptosis in ARPE-19 cells after 6 hours of blue light exposure, characterized by increased expression of ferroptosis-related factors (NCOA4, FTH1, FTL, SLC39A14, LPCAT3, HMOX1, SLC7A11, P53) and decreased expression of SLC3A2 and GPX4. Proteins CCNB1, MCM4, MCM2, and CDC6 were implicated in the damage induced by 6 hours of blue light irradiation, whereas IL-1β, EGR1, DDIT3, and HSPA1A emerged as crucial players in the damage induced by 12 hours of blue light exposure. These findings underscore the detrimental impact of blue light on ARPE-19 cells, shedding light on alterations in Differentially Expressed Genes (DEGs) that contribute to understanding the potential ocular hazards associated with blue light. This knowledge forms the basis for the safe application of blue light and provides a potential therapeutic target for retinal degenerative diseases induced by blue light. Future research aims to validate immune signaling pathways triggered by blue light-induced oxidative stress in RPE cells, particularly the ferroptosis signaling pathway and its key regulators. The goal is to identify targeted drugs that may reverse blue light-induced apoptosis or cell death, ultimately preventing and treating retinal damage caused by blue light exposure.

Acknowledgments*:*

This research was funded by the National Natural Science Foundation of China grant number 81901907.

Competing Interests

The authors have declared that no competing interests exist.

References

1. Li, B., W. Zhang, Z. Li and B. Guo (2018) Research on application of LED navaid lighting in airfield area of civil airports. *IOP Conference Series: Materials Science and Engineering.* **392**, 062109.
2. Shih-Chang, H. and T. Sung-Keng (2022) High-power buck chip design for vehicle far/near headlights. *Analog. Integr. Circ. Sig. Process.***111**, 1-11.
3. Wang, S., D. Su and Y. Wu (2022) Environmental and social life cycle assessments of an industrial LED lighting product. *Environ. Impact Assess. Rev.* **95**, 106804.
4. Hatori, M., C. Gronfier, R.N. Van Gelder, P.S. Bernstein, J. Carreras, S. Panda, F. Marks, D. Sliney, C.E. Hunt, T. Hirota, T. Furukawa and K. Tsubota (2017) Global rise of potential health hazards caused by blue light-induced circadian disruption in modern aging societies. *NPJ. Aging. Mech. Dis*. **3**, 9.
5. Shang, Y.M., G.S. Wang, D.H. Sliney, C.H. Yang and L.L. Lee (2017) Light-emitting-diode induced retinal damage and its wavelength dependency in vivo. Int. J. Ophthalmol. 10(2), 191-202.
6. Jaadane, I., P. Boulenguez, S. Chahory, S. Carré, M. Savoldelli, L. Jonet, F. Behar-Cohen, C. Martinsons and A. Torriglia (2015) Retinal damage induced by commercial light

emitting diodes (LEDs). Free. Radic. Biol. Med. 84, 373-384.
7. Touitou, Y. and S. Point (2020) Effects and mechanisms of action of light-emitting diodes on the human retina and internal clock. Environ. Res. 190, 109942.
8. Vila, N., A. Siblini, E. Esposito, V. Bravo-Filho, P. Zoroquiain, S. Aldrees, P. Logan, L. Arias and M.N. Burnier (2017) Blue-light filtering alters angiogenic signaling in human retinal pigmented epithelial cells culture model. BMC. Ophthalmol. 17(1), 198.
9. Liu, X., Q. Zhou, H. Lin, J. Wu, Z. Wu, S. Qu and Y. Bi (2019) The protective effects of blue light-blocking films with different shielding rates: a rat model study. Transl. Vis. Sci. Technol. 8(3), 19.
10. Zheng, Q.X., Y.P. Ren, P.S. Reinach, B. Xiao, H.H. Lu, Y.R. Zhu, J. Qu and W. Chen (2015) Reactive oxygen species activated NLRP3 inflammasomes initiate inflammation in hyperosmolarity stressed human corneal epithelial cells and environment-induced dry eye patients. *Exp Eye Res.* **134**, 133-140.
11. Babizhayev, M.A. (2011) Mitochondria induce oxidative stress, generation of reactive oxygen species and redox state unbalance of the eye lens leading to human cataract formation: disruption of redox lens organization by phospholipid hydroperoxides as a common basis for cataract disease. *Cell. Biochem. Funct.* **29**(3), 183-206.
12. Zhao, Z.C., Y. Zhou, G. Tan and J. Li (2018) Research progress about the effect and prevention of blue light on eyes. *Int J Ophthalmol.* **11**, 1999-2003.
13. Hoon, M., H. Okawa, L.D. Santina and R.O. Wong (2014) Functional architecture of the retina: development and disease. *Prog. Retin. Eye. Res.* **42**, 44-84.
14. George, S.M., F. Lu, M. Rao, L.L. Leach and J.M. Gross (2021) The retinal pigment epithelium: development, injury responses, and regenerative potential in mammalian and non-mammalian systems. *Prog. Retin. Eye. Res.* **85**, 100969.
15. Chiba, C (2014) The retinal pigment epithelium: an important player of retinal disorders and regeneration. *Exp. Eye. Res.* **123**, 107-114.
16. Lin, Y.H., S.J. Sheu, W. Liu, Y.T. Hsu, C.X. He, C.Y. Wu, K.J. Chen, P.Y. Lee, C.C. Chiu and K.C. Cheng (2023) Retinal protective effect of curcumin metabolite hexahydrocurcumin against blue light-induced RPE damage. *Phytomedicine*. **110**, 154606.
17. Wu, J., S. Seregard and P.V. Algvere (2006) Photochemical damage of the retina. *Surv. Ophthalmol.* **51**(5), 461-481.
18. Zrenner, E (1990) Light-induced damage to the eye. *Fortschr. Ophthalmol.* **87**(Suppl), S41-51.
19. Moon, J., J. Yun, Y.D. Yoon, S.I. Park, Y.J. Seo, W.S. Park, H.Y. Chu, K.H. Park, M.Y. Lee, C.W. Lee, S.J. Oh, Y.S. Kwak, Y.P. Jang and J.S. Kang (2017) Blue light effect on retinal pigment epithelial cells by display devices. *Integr. Biol (Camb).* **9**(5), 436-443.
20. Cougnard-Gregoire, A., B.M.J. Merle, T. Aslam, J.M. Seddon, I. Aknin, C.C.W. Klaver, G. Garhöfer, A.G. Layana, A.M. Minnella, R. Silva and C. Delcourt (2023) Blue light exposure: ocular hazards and prevention-a narrative review. *Ophthalmol. Ther.* **12**(2), 755-788.
21. Brandstetter, C., Patt, J., F.G. Holz and T.U. Krohne (2016) Inflammasome priming increases retinal pigment epithelial cell susceptibility to lipofuscin phototoxicity by changing the cell death mechanism from apoptosis to pyroptosis. *J. Photochem. Photobiol. B.* **161**, 177-183.
22. Sun, Y., Y.F Zheng and Y.Z. Liu (2018) Ferroptosis involves in excessive light induced damage of retinal pigment epithelium. *Invest. Ophthalmol. Vis. Sci*. **59**, 2482.
23. Zhou, B., J. Liu, R. Kang, D.J. Klionsky, G. Kroemer and D. Tang (2020) Ferroptosis is a type of autophagy-dependent cell death. *Semin. Cancer. Biol.* **66**, 89-100.
24. Yu, H., C. Yang, L. Jian, S. Guo, R. Chen, K. Li, F. Qu, K. Tao, Y. Fu, F. Luo and S. Liu (2019) Sulfasalazine-induced ferroptosis in breast cancer cells is reduced by the inhibitory effect of estrogen receptor on the transferrin receptor. *Oncol. Rep.* **42**(2), 826-838.
25. W.S. Yang, K.J. Kim, M.M. Gaschler, M. Patel, M.S. Shchepinov and B.R. Stockwell (2016) Peroxidation of polyunsaturated fatty acids by lipoxygenases drives ferroptosis.

Proc. Natl. Acad. Sci. U S A. **113**(34), E4966-4975.
26. Yang, J., X. Dai, H. Xu, Q. Tang and F. Bi (2022) Regulation of ferroptosis by amino acid metabolism in cancer. *Int. J. Biol. Sci.* **18**(4), 1695-1705.
27. Bersuker, K., J.M. Hendricks, Z. Li, L. Magtanong, B. Ford, P.H. Tang, M.A. Roberts, B. Tong, T.J. Maimone, R. Zoncu, M.C. Bassik, D.K. Nomura, S.J. Dixon and J.A. Olzmann (2019) The CoQ oxidoreductase FSP1 acts parallel to GPX4 to inhibit ferroptosis. *Nature.* **575**(7784), 688-692.
28. Alim, I., J.T. Caulfield, Y. Chen, V. Swarup, D.H. Geschwind, E. Ivanova, J. Seravalli, Y. Ai, L.H. Sansing, E.J. Ste Marie, R.J. Hondal, S. Mukherjee, J.W. Cave, B.T. Sagdullaev, S.S. Karuppagounder and R.R. Ratan (2019) Selenium drives a transcriptional adaptive program to block ferroptosis and treat stroke. *Cell.* **177**(5), 1262-1279.e25.
29. Imai, H., M. Matsuoka, T. Kumagai, T. Sakamoto and T. Koumura (2017) Lipid peroxidation-dependent cell death regulated by GPx4 and ferroptosis. *Curr. Top. Microbiol. Immunol.* **403**, 143-170.
30. Chen, C., J. Chen, Y. Wang, Z. Liu and Y (2021) Wu. Ferroptosis drives photoreceptor degeneration in mice with defects in all-trans-retinal clearance. *J. Biol. Chem.* **296**, 100187.
31. Li, X., S. Zhu and F. Qi (2023) Blue light pollution causes retinal damage and degeneration by inducing ferroptosis. *J. Photochem. Photobiol. B.* **238**, 112617.
32. Miralles de Imperial-Ollero, J.A., A. Gallego-Ortega, A. Ortín-Martínez, M.P. Villegas-Pérez, F.J. Valiente-Soriano and M. Vidal-Sanz (2021) Animal models of LED-induced phototoxicity. Short- and long-term in vivo and ex vivo retinal alterations. *Life (Basel).* **11**(11), 1137.
33. Yang, S., J. Zhou and D. Li (2021) Functions and diseases of the retinal pigment epithelium. *Front. Pharmacol.* **12**, 727870.
34. Withanage, M.H.H., H. Liang and E. Zeng (2022) RNA-seq experiment and data analysis. *Methods. Mol. Biol.* **2418**, 405-42.
35. Wang, L., Y. Xin, D. Zhang, Y. Wen, L. Zhang, Y. Xia, J. Chen, C. Xie, H. Zhu, J. Tong and Y. Shen (2023) Long-term blue light exposure impairs mitochondrial dynamics in the retina in light-induced retinal degeneration in vivo and in vitro. *J. Photoch. Photobio. B.* **240**, 112654.
36. Xie, C., H. Zhu, S. Chen, Y. Wen, L. Jin, L. Zhang, J. Tong and Y. Shen (2020) Chronic retinal injury induced by white LED light with different correlated color temperatures as determined by microarray analyses of genome-wide expression patterns in mice. *J. Photochem. Photobiol. B.* **210**, 111977.
37. Tang, Z., Y. Ju, X. Dai, N. Ni, Y. Liu, D. Zhang, H. Gao, H. Sun, J. Zhang and P. Gu (2021) HO-1-mediated ferroptosis as a target for protection against retinal pigment epithelium degeneration. *Redox. Biol.* **43**, 101971.
38. Rochette, L., G. Dogon, E. Rigal, M. Zeller, Y. Cottin and C. Vergely (2022) Lipid peroxidation and iron metabolism: two corner stones in the homeostasis control of ferroptosis. *Int. J. Mol. Sci.* **24**(1), 449.
39. Wu, H., Q. Liu, X. Shan, W. Gao and Q. Chen (2023) ATM orchestrates ferritinophagy and ferroptosis by phosphorylating NCOA4. *Autophagy*. **19**(7), 2062-2077.
40. Zhang, Y., X. Wu, J. Zhu, R. Lu and Y (2023) Ouyang. Knockdown of SLC39A14 inhibits glioma progression by promoting erastin-induced ferroptosis SLC39A14 knockdown inhibits glioma progression. *BMC. Cancer.* **23**(1), 1120.
41. Gao, M., P. Monian, N. Quadri, R. Ramasamy and X. Jiang (2015) Glutaminolysis and transferrin regulate ferroptosis. *Mol. Cell.* **59**(2), 298-308.
42. Ingold, I., C. Berndt, S. Schmitt, S. Doll, G. Poschmann, K. Buday, A. Roveri, X. Peng, F. Porto Freitas, T. Seibt, L. Mehr, M. Aichler, A. Walch, D. Lamp, M. Jastroch, S. Miyamoto, W. Wurst, F. Ursini, E.S.J. Arnér, N. Fradejas-Villar, U. Schweizer, H. Zischka, J.P. Friedmann Angeli and M. Conrad (2018) Selenium utilization by GPX4 is required to prevent hydroperoxide-induced ferroptosis. *Cell*. **172**(3), 409-422.e21.
43. Xue, Q., D. Yan, X. Chen, X. Li, R. Kang, D.J. Klionsky, G. Kroemer, X. Chen, D. Tang and J. Liu (2023) Copper-dependent autophagic degradation of GPX4 drives ferroptosis. *Autophagy*. **19**(7), 1982-1996.
44. Rochette, L., G. Dogon, E. Rigal, M. Zeller, Y. Cottin and C. Vergely (2022) Lipid

peroxidation and iron metabolism: two corner stones in the homeostasis control of ferroptosis. *Int. J. Mol. Sci*. **24**(1), 449.
45. Ma, Q., T. Xu and H. Kang (2023) A Study on the necroptosis of ARPE-19 cells induced by 448 nm blue light. *Acta. Laser. Biology. Sinica.* **32**(1), 36-42 (in Chinese).
46. Song, W., R. Zhu, W. Gao, C. Xing and L.Yang (2022) Blue light induces RPE cell necroptosis, which can be inhibited by minocycline. *Front. Med. (Lausanne).* **9**, 831463.
47. Hu, L. and G. Xu (2021) Potential protective role of TRPM7 and involvement of PKC/ERK pathway in blue light-induced apoptosis in retinal pigment epithelium cells in vitro. *Asia. Pac. J. Ophthalmol. (Phila).* **10**(6), 572-578.
48. Lin, C., M. Wu, C. Li, H. Cheng, S. Huang, C. Tsai, F. Lin, J. Ho, J. Kang, G. Hsiao and Y. Cheng (2017) Periodic exposure to ssmartphone-mimic low-luminance blue light induces retina damage through Bcl-2/BAX-dependent apoptosis. *Toxicol. Sci.* **157**(1), 196–210.
49. Lascaratos, G., D. Ji, J.P. Wood and N.N. Osborne (2007) Visible light affects mitochondrial function and induces neuronal death in retinal cell cultures. *Vision. Res.* **47**(9), 1191-1201.
50. Sparrow, J.R. and B. Cai (2001) Blue light-induced apoptosis of A2E-containing RPE: involvement of caspase-3 and protection by Bcl-2. *Invest. Ophthalmol. Vis. Sci.* **42**(6), 13 56-1362.
51. Marie, M., K. Bigot, C. Angebault, C. Barrau, P. Gondouin, D. Pagan, S. Fouquet, T. Villette, J.A. Sahel, G. Lenaers and S. Picaud (2018) Light action spectrum on oxidative stress and mitochondrial damage in A2E-loaded retinal pigment epithelium cells. *Cell. Death. Dis.* **9**(3), 287.
52. Cho, H.M., S.J. Lee and S.Y. Choung (2023) Protective effects of Panax ginseng berry extract on blue light-induced retinal damage in ARPE-19 cells and mouse retina. *J Ginseng Res.* **47**(1), 65-73.
53. Grzelak, A., B. Rychlik and G. Bartosz (2001) Light-dependent generation of reactive oxygen species in cell culture media. *Free. Radic. Biol. Med.* **30**(12), 1418-1425.